Sum Rate Maximization of Uplink Active RIS and UAV-assisted THz Mobile Communications

Sara Farrag
German University in Cairo
sarah.farrag@guc.edu.eg

Engy A. Maher
German University in Cairo
engy.maher@guc.edu.eg

Ahmed El-Mahdy
German University in Cairo
ahmed.elmahdy@guc.edu.eg

Falko Dressler
TU Berlin
dressler@ccs-labs.org

***Abstract*—Terahertz (THz) band communication is considered as a key technology for 6G and beyond. THz communication can boost plethora of promising applications. Wireless communication systems for unmanned aerial vehicle (UAV) promises to provide cost-effective wireless connectivity without infrastructure coverage. As a supporting element, an active reconfigurable intelligent surface (RIS) can be used such that both phase shifts and amplitudes of its elements are tuned to create favorable beam steering, such that undesired interference from other devices is mitigated. In this paper, we consider a UAV equipped with an active RIS operating in THz band, where a cellular user as well as a number of co-existing device-to-device (D2D) links are considered. We assume that direct paths between each two communicating nodes are not available. Only the RIS-reflected paths are considered. We propose a joint power allocation and active RIS precoding matrix optimization scheme to maximize the sum rate. The proposed scheme is evaluated in terms of the achieved sum rate and compared with passive RIS and multi-antenna amplify-and-forward (AF) relaying. Numerical results show that the proposed active RIS-aided approach is superior to the other schemes, achieving the highest sum rate.**

***Index Terms*—Wireless communication, Reliable Communication, Sum Rate, UAV, THz, active RIS and D2D.**

I. Introduction

While wireless communications have progressed significantly towards 5G: systems capacities has been remarkably increased by evolving the transceiver design, while the wireless channel has always been considered uncontrollable [1]. Lately, due to the advances in meta-materials, deploying reconfigurable intelligent surfaces in wireless networks has been suggested for the sake of intelligently controlling wireless channels in a desired manner [2], [3]. Generally, RIS is an array of passive reflecting elements, where each element can be independently tuned to induce a phase shift to the incident signal [4]. Because of its low cost, small size, light weight and convenient deployment, RIS can be deployed in today's wireless networks for the sake of achieving a higher sum rate [5]. By optimizing the phase shifts of the RIS, the signals transmitted via the reflecting channel link can be constructively added at intended receiving user or destructively added at the interferer, resulting in a higher rate than that in case of without RIS. On the other hand, the conventional passive RIS can only reflect the incident signal without introducing any gain. In addition, the capacity gain introduced by passive RIS is limited due to "multiplicative fading" effect that is remarkable in communication scenarios implying strong line-of-sight (LOS) links between the base station (BS) and the users [6]. To solve this issue, active RIS has been introduced to simultaneously amplify the incident electromagnetic signal and favorably adjust its phase shift. Compared to AF relays, the active RIS operates in the full-duplex (FD) mode and is equipped with low-power-reflection-type amplifiers rather than having power-hungry-radio frequency chains [7].

Thanks to their flexible maneuverability with the fully controllable UAV's position in three dimensional (3D) airspace and convenient deployment, UAVs are considered an effective solution to achieve temporary wireless connectivity [8]. With their inherent mobility and flexibility capabilities, UAVs can provide higher wireless capacity, more reliability, better coverage and higher energy efficient–systems [9]. In addition, UAVs are a key to numerous potential applications in wireless systems, specially in areas that exhibits no or limited terrestrial infrastructure. Compared to other airborne solutions such as high altitude platforms, implementing UAV-enabled wireless communication has various advantages compared to terrestrial BSs as UAVs are always on-demand and can be easily deployed in any already existing network [10]. In addition, UAV–enabled wireless communication are characterized by its offered superior link quality in the presence of shorter distance LOS communication channels with communicating ground nodes [11].

Examining the spectrum below 6 GHz, it is found exploited, congested and in excessive use by WiFi, broadcasting, satellites and other existing communication networks [12]. With deploying communication systems in the THz frequency band (ranging from 0.1 THz to 10 THz), terabit-per-second (Tbps) links are expected to be reality within the few upcoming years [13]. Thanks to its promising ultra wide bandwidth (BW), high throughput, low latency and seamless data transfer rate, THz has recently received great attention within the decision makers and research communities [14]. Furthermore, the THz waves are more suitable candidates for uplink communication. Specially, they allow non–line–of–sight (NLOS) propagation and act as reliable substitutes during inconvenient climate conditions such as rain, turbulence, dust and fog [15]. On the other hand, the excessive available bandwidth THz offers comes always at the

This work is supported by the DAAD and in part by the Federal Ministry of Education and Research (BMBF, Germany) within the 6G Research and Innovation Cluster 6G-RIC under Grant 16KISK020K, in co-operation between the department of telecommunications systems at TU Berlin and German University in Cairo.

expense of high propagation loss. In fact, this substantial loss is arisen while the electromagnetic wave propagates through the medium and also due to the absorption loss caused by the molecular absorption in water vapor molecules existing in the atmosphere [16].

II. Related Work

There are few papers concerning sum rate maximization for active RIS-assisted networks over the THz channel in uplink communication. The authors in [17] proposed a dynamic RIS sub-array structure to improve the performance of a THz downlink multiple-input-multiple-output (MIMO) communication system. In their work, weighted minimum mean square error - RIS local search (WMMSE-LS) scheme with limited RIS phase shift accuracy and an adaptive BCD-aided joint beamforming approach were proposed to improve throughput performance for the investigated RIS THz system. In [18], a hybrid beamforming scheme for the multi-hop RIS-assisted communication networks is proposed to improve the coverage range at THz-band frequencies. The joint design of digital beamforming matrix at the BS as well as analog beamforming matrices at the RIS are dealt with using deep reinforcement learning (DRL) to combat the propagation loss.

From the above discussions, it is noted that researchers did not yet focus on analyzing the sum rate of the uplink of mobile device to BS through a UAV equipped with an active RIS in the THz channel in the presence of underlying D2D pairs. In this paper, we tackle specifically this problem. Our main contributions can be summarized as follows:

- A UAV equipped with an active RIS aided network in THz band is considered. A cellular user link and a number of D2D links are established through reflected paths supported by active RIS reflected paths between each two communicating nodes. Consequently, the transmitting power of each transmitting node as well as the amplitudes and phase shifts of the active RIS reconfigurable elements are studied.
- A joint power allocation and active RIS precoding matrix optimization scheme is proposed to maximize the sum rate of the scenario under consideration. The objective function is found non-convex. Then, fractional programming methods are proposed. Since the transmitting powers and phase shifts are independent of each other, we decouple the joint optimization problem into two sub-problems: the transmitting power allocation sub-problem and active RIS precoding matrix optimization sub-problem.
- For the active RIS precoding matrix optimization problem, it is formulated as a quadratic constraint quadratic programming (QCQP) problem and is solved using Lagrangian multiplier method. For the transmitting powers optimization sub-problem, it is also formulated as a QCQP problem and is solved using CVX.
- Simulations are performed and numerical values are obtained to compare our proposed scheme for active RIS with the performance in the case deploying passive RIS as well as in the case of deploying multi-antenna AF relaying scheme. The proposed scheme is proven to outperform its counterparts from the literature, achieving higher sum rates in different scenarios.

Notations: $[.]^{-1}$, $[.]^T$ and $[.]^H$ denote the inverse, transpose and Hermitian operations, respectively. $\|.\|$ denotes the Frobenius norm and $\otimes$ denotes the Kronecker product. $\mathbb{C}$, $\mathbb{R}$ and $\mathbb{R}_+$ denote the set of complex, real and positive real numbers, respectively. $\boldsymbol{I_N}$ and $\boldsymbol{0_N}$ denote an identity $N \times N$ matrix and $1 \times N$ zero vector, respectively.

III. System and Channel Model

A. System Model

The system under consideration consists of a single cell cellular active RIS-aided network as shown in Fig. 1. As shown in the Figure, the system consists of one mobile device (MD), one UAV, one BS and M D2D pairs that coexist and are assigned the same frequency resources as the MD. In fact, the uplink communication between the MD and the BS and the link between any D2D pair is established with the support of a UAV equipped with an active RIS. Simultaneously, the RIS supports a number of D2D pairs that have the same frequency with the MD. It is assumed that the number of D2D pairs is M. Consequently, a total of $Q = M + 1$ links exist in the system. For any link, it is assumed that the direct transmission link between any two communicating nodes is unattainable due to high loss resulting from long distances travelled or the existence of obstacles. Therefore, only RIS-based reflected link can be established to strengthen the received signals. Interference exists among all links and cannot be neglected, which is a vital issue that limits the system performance. The RIS is an $N \times N$ uniform planar array, where it consists of N^2 reconfigurable

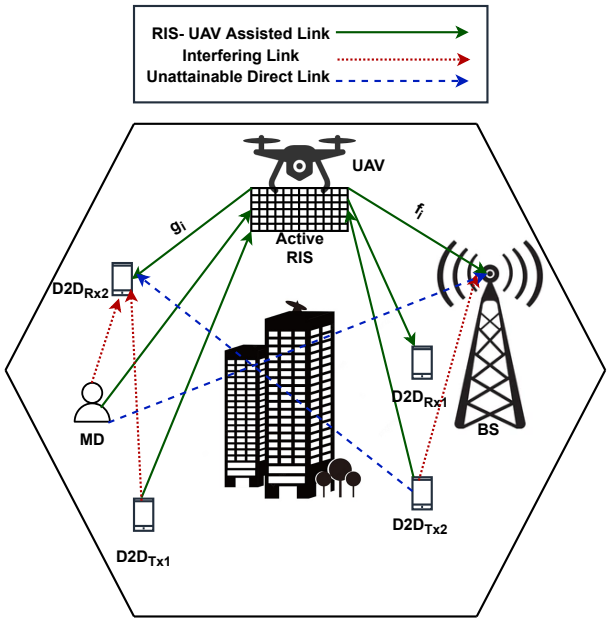

Fig. 1: Scenario considering a UAV equipped with an active RIS that is deployed to assist the communication link between the MD and the BS as well as between D2D pairs.

great quality built-in programmable elements which their phases and amplitudes are smartly tuned by varactor diodes. In other words, favorable phase shift and amplitude is provided by the metal plate to mitigate interference among the communication links and enhance the system performance. In addition, we deploy this RIS on a UAV to enhance the adaptability of the system. However, just for simplicity, we assume we have a fixed-positioned UAV for the provided analysis.

The channels between the communication nodes in the network are considered to be THz channels. It is assumed that the channels between the nodes are known or at least can be perfectly estimated. The description of this channel is provided in the next subsection.

B. Channel Model

In this sub-section, the THz channel model is elaborated. It was derived using THz wave atmospheric transmission attenuation model and water vapour absorption that mainly characterize the THz band. The THz channel gain is formulated as [9], [16] and is expressed as

$$h_{Thz} = \sqrt{\frac{1}{PL(f,d)}}, \tag{1}$$

where $PL(f,d)$ is the pathloss that frequency f suffers when propagating a distance d. $PL(f,d)$ accounts for spreading loss $L_{sl}(f,d)$ as well as molecular absorption $L_{mal}(f,d)$ that distinguishes the THz frequency band. The spreading loss $L_{sl}(f,d)$ is resulting from the expansion of the electromagnetic wave when it propagates through unlike mediums. On the other hand, the molecular absorption $L_{mal}(f,d)$ is a consequent of the collisions between water molecules and/or atmospheric gas. Detailed study for the effect of atmospheric attenuation was carried out in [19].

The channel coefficient h_{THz} follows zero-mean complex Gaussian distribution, having a variance that models free space path and molecular absorption gain. From [19] (Eqn. (2), (3) and (5)), the pathloss experienced at frequency f after propagating a distance d is a function of the variance of the THz channel and is given as

$$PL(f,d) = \frac{1}{\sigma^2} = \frac{1}{G_{Tx}G_{Rx}}(\frac{4\pi f d}{c})^2 e^{k(f)d}, \tag{2}$$

where σ^2 is the variance of the THz channel which has zero mean. So, $h_{THz} \sim CN(0,\sigma^2)$. G_{Tx} and G_{Rx} are the gains of the transmitter and receiver antennas, respectively. c is the speed of light in free space and $k(f)$ represents the frequency dependent medium absorption factor and is given in [20].

IV. Mathematical Formulation

The received signal at any receiver i can be expressed as

$$\begin{aligned} y_i = &\underbrace{\boldsymbol{f}_i^H \boldsymbol{\Phi} \boldsymbol{g}_i a_i x_i}_{\text{Desired Signal}} + \sum_{\substack{j=1 \\ j\neq i}}^{Q} \underbrace{\boldsymbol{f}_i^H \boldsymbol{\Phi} \boldsymbol{g}_j a_j x_j}_{\text{Interference links}} \\ &+ \underbrace{\boldsymbol{f}_i^H \boldsymbol{\Phi} \boldsymbol{v}}_{\text{Dynamic noise}} + \underbrace{n_o}_{\text{AWGN noise}} ; \end{aligned} \tag{3}$$

where $\boldsymbol{f}_i \in \mathbb{C}^{N\times 1}$ denotes the channel vector between the RIS and receiver i, $\boldsymbol{\Phi} \in \mathbb{C}^{N\times N}$, $\boldsymbol{\Phi}$ = diag $[\eta_1 e^{j\theta_1}, ..., \eta_N e^{j\theta_N}]^H$ is the precoding matrix of the active RIS coefficients (i.e., phase shifts and amplitudes), where $\theta_n \in [\ 0, 2\pi)$ and $\boldsymbol{g}_i \in \mathbb{C}^{N\times 1}$ is the channel vector between transmitter i and the RIS, a_i is the transmitting amplitude of transmitting device i where $a = [a_1, ..., a_Q]$, x_i is the transmitting signal of the MD and has unit energy, $\boldsymbol{v}$ is related to the input noise as well as inherent device noise of active RIS elements $v \sim \mathcal{CN}(\boldsymbol{0_N}, \sigma_v^2 \boldsymbol{I_N})$. This noise is not found in passive RIS [1] and n_o denotes the additive white Gaussian noise (AWGN) which has zero mean and variance N_o.

Using (3), the achieved SINR at receiver i is expressed as

$$\gamma_i = \frac{|\boldsymbol{f}_i^H \boldsymbol{\Phi} \boldsymbol{g}_i a_i|^2}{\sum_{\substack{j=1 \\ j\neq i}}^{Q} |\boldsymbol{f}_i^H \boldsymbol{\Phi} \boldsymbol{g}_j a_j|^2 + ||\boldsymbol{f}_i^H \boldsymbol{\Phi}||^2 \sigma_v^2 + N_o}. \tag{4}$$

The maximum power budget assigned to the active RIS $P_{RIS_{max}}$ can be written as

$$P_{RIS_{max}} = \sum_{i=1}^{Q} ||\boldsymbol{\Phi} \boldsymbol{g}_i a_i||^2 + ||\boldsymbol{\Phi}||^2 \sigma_v^2. \tag{5}$$

Therefore, the original problem of sum rate maximization, subject to power constraints at the active RIS $P_{RIS_{max}}$ and available transmitting nodes' power $P_{T_{max}}$ is formulated as

$$\max_{\boldsymbol{\Phi}, \boldsymbol{a}} W \sum_{i=1}^{Q} log_2(1+\gamma_i), \tag{6a}$$

$$s.t. \sum_{i=1}^{Q} ||\boldsymbol{\Phi} \boldsymbol{g}_i a_i||^2 + ||\boldsymbol{\Phi}||^2 \sigma_v^2 \leq P_{RIS_{max}}, \tag{6b}$$

$$\sum_{i=1}^{Q} a_i^2 \leq P_{T_{max}} \tag{6c}$$

$$0 \leq a_i, \forall i = 1, ..., Q. \tag{6d}$$

where W represents the system assigned BW and $P_{T_{max}}$ is the maximum power that can be assigned to the MD or any transmitting D2D device.

Solving the optimization problem given in (6) is a challenging task due to its non-convexity. In order to efficiently solve this problem, a joint power allocation and active RIS precoding matrix optimization scheme based on fractional programming is proposed in the next Section.

V. Proposed Power Allocation and RIS Precoding Matrix Optimization Algorithm

In this section, we solve the rate maximization problem given in (6). In other words, we aim at obtaining the optimum power of transmitting nodes $\boldsymbol{a}$ and the optimum active RIS precoding matrix $\boldsymbol{\Phi}$. It is noticed that the objective function in (6) is non-convex sum of logarithms and fractions. Consequently, fractional programming methods are used. According to the

Lemma presented in [21], the optimization problem presented in (6) can be formulated as

$$\max_{\boldsymbol{\Phi},\boldsymbol{a},\boldsymbol{\zeta},\boldsymbol{\kappa}} R_{sum}(\boldsymbol{\Phi},\boldsymbol{a},\boldsymbol{\zeta},\boldsymbol{\kappa}) = W\Big[\sum_{i=1}^{Q} ln(1+\zeta_i) - \sum_{i=1}^{Q}\zeta_i + \sum_{i=1}^{Q}\beta(\boldsymbol{\Phi},\boldsymbol{a},\boldsymbol{\zeta},\boldsymbol{\kappa})\Big] \tag{7a}$$

$$s.t. \sum_{i=1}^{Q} ||\boldsymbol{\Phi}\boldsymbol{g}_i a_i||^2 + ||\boldsymbol{\Phi}||^2\sigma_v^2 \leq P_{RIS_{max}}. \tag{7b}$$

where $\beta(\boldsymbol{\Phi},\boldsymbol{\zeta_i},\boldsymbol{\kappa_i})$ is given as:

$$\beta(\boldsymbol{\Phi},\boldsymbol{a},\boldsymbol{\zeta_i},\boldsymbol{\kappa_i}) = 2\sqrt{1+\zeta_k}\Re\{\kappa_i^*(\boldsymbol{f}_i^H\boldsymbol{\Phi}\boldsymbol{g}_i)^H a_i\} - |\kappa_i|^2\Big(\sum_{\substack{j=1\\j\neq i}}^{Q}|(\boldsymbol{f}_i^H\boldsymbol{\Phi}\boldsymbol{g}_j)a_j|^2 + ||\boldsymbol{f}_i^H\boldsymbol{\Phi}||^2\sigma_v^2 + N_o\Big); \tag{8}$$

where auxiliary variables $\boldsymbol{\zeta} := [\zeta_1,....,\zeta_Q] \in \mathbb{R}_+^{\mathbb{Q}}$ and $\boldsymbol{\kappa} := [\kappa_1,....,\kappa_Q] \in \mathbb{C}^{\mathbb{Q}}$ are introduced above. In (8), strong convergence of the fractional programming method was proven. Hence, a locally optimal solution of (7) is obtained by alternately optimizing the active RIS precoding matrix $\boldsymbol{\Phi}$, MD and D2Ds transmitting powers $\boldsymbol{a}$ and auxiliary variables ζ_i and κ_i. In other words, obtaining one variable and fixing the other three.

Optimize $\boldsymbol{\zeta}$ and fix ($\boldsymbol{\Phi}$, $\boldsymbol{\kappa}$, $\boldsymbol{a}$)

By fixing RIS precoding matrix, auxiliary variable $\boldsymbol{\kappa}$ and the transmitting amplitudes $\boldsymbol{a}$, the optimal ζ_i is obtained by differentiating (7a) w.r.t. ζ_i and equating to zero. This results in

$$\frac{\partial R_{sum}(\boldsymbol{\Phi},\boldsymbol{a},\boldsymbol{\zeta},\boldsymbol{\kappa})}{\partial\zeta_i} = \frac{1}{1+\zeta i} - 1 + \frac{1}{\sqrt{1+\zeta i}}\lambda_i = 0; \tag{9}$$

where

$$\lambda_i = \Re\{\kappa_i^*(\boldsymbol{f}_i^H\boldsymbol{\Phi}\boldsymbol{g}_i)^H a_i\}. \tag{10}$$

After some simplifications and mathematical manipulations, ζ_i^{opt} is obtained as:

$$\zeta_i^{opt} = \frac{\lambda_i^2 + \lambda_i\sqrt{\lambda_i^2+4}}{2}, \forall i \in \{1,2,...,Q\}. \tag{11}$$

Optimize $\boldsymbol{\kappa}$ and fix ($\boldsymbol{\Phi}$, $\boldsymbol{a}$, $\boldsymbol{\zeta}$)

By fixing the RIS precoding matrix $\boldsymbol{\Phi}$, the transmitting amplitudes $\boldsymbol{a}$ and auxiliary variable $\boldsymbol{\zeta}$, the optimal κ_i is obtained by differentiating (7a) w.r.t. κ_i and equating to zero. Hence, the following holds

$$\frac{R_{sum}(\boldsymbol{\Phi},\boldsymbol{a},\boldsymbol{\zeta},\boldsymbol{\kappa})}{\partial\kappa_i} = 2\sqrt{1+\zeta_i}(\boldsymbol{f}_i^H\boldsymbol{\Phi}\boldsymbol{g_i})^H a_i - 2\kappa_i(\sum_{\substack{j=1\\j\neq i}}^{Q}|(\boldsymbol{f}_i^H\boldsymbol{\Phi}\boldsymbol{g}_j)^H a_j|^2 + ||\boldsymbol{f}_i^H\boldsymbol{\Phi}||^2\sigma_v^2 + N_o) = 0. \tag{12}$$

Then, κ_i^{opt} is obtained as

$$\kappa_i^{opt} = \frac{\sqrt{1+\zeta_i}(\boldsymbol{f}_i^H\boldsymbol{\Phi}\boldsymbol{g}_i)^H a_i}{\sum_{\substack{j=1\\j\neq i}}^{Q}|(\boldsymbol{f}_i^H\boldsymbol{\Phi}\boldsymbol{g}_j)^H a_j|^2 + ||\boldsymbol{f}_i^H\boldsymbol{\Phi}||^2\sigma_v^2 + N_o} \tag{13}$$

Optimize $\boldsymbol{\Phi}$ and fix ($\boldsymbol{\zeta}$, $\boldsymbol{\kappa}$, $\boldsymbol{a}$)

The maximization problem in (7) can be reformulated as

$$\max_{\boldsymbol{\phi}} \Re\{\boldsymbol{B}\boldsymbol{\phi}\} - \boldsymbol{\phi}^H\boldsymbol{\Delta}\boldsymbol{\phi}, \tag{14a}$$

$$s.t. \boldsymbol{\phi}^H\boldsymbol{\Lambda}\boldsymbol{\phi} \leq P_{RIS_{max}}, \tag{14b}$$

where

$$\boldsymbol{B} = 2\Big(\sum_{i=1}^{Q}\sqrt{1+\zeta_i}\kappa_i^* a_i\boldsymbol{f}_i^H diag(\boldsymbol{g}_i)\Big); \tag{15}$$

$$\boldsymbol{\Delta} = \sum_{i=1}^{Q}|\kappa_i|^2 diag(\boldsymbol{f_i}^H)diag(\boldsymbol{f_i})\sigma_v^2 + \sum_{i=1}^{Q}|\kappa_i|^2\sum_{\substack{j=1\\j\neq i}}^{Q}a_j^2 diag(\boldsymbol{g_j}^H)\boldsymbol{f}_i\boldsymbol{f}_i^H diag(\boldsymbol{g_j}); \tag{16}$$

$$\boldsymbol{\Lambda} = \sum_{i=1}^{Q}a_i^2 diag(\boldsymbol{g_i})(diag(\boldsymbol{g_i}))^H + \sigma_v^2\boldsymbol{I}_N. \tag{17}$$

It is noted that (14) is a QCQP problem. Thus, using the Lagrangian multiplier method, the optimal solution $\boldsymbol{\phi}^{opt}$ is obtained and is given as

$$\boldsymbol{\phi}^{opt} = (\boldsymbol{\Delta} + \mu\boldsymbol{\Lambda})^{-1}\boldsymbol{B}^H, \tag{18}$$

where the optimal Lagrange multiplier μ^{opt} is obtained using binary search method. Algorithm 1 summarizes the Lagrangian multiplier method used to solve (14), where binary search method is involved. It starts with initializing lower and upper limits of the Lagrangian multiplier, μ^l and μ^u, respectively. Accordingly, two values of $\boldsymbol{\phi}$ are obtained by substituting with μ^l and μ^u in (18), namely $\boldsymbol{\phi}^l$ and $\boldsymbol{\phi}^u$, respectively. As Algorithm 1 illustrates, conditions are evaluated till the optimum μ is obtained and accordingly, $\boldsymbol{\phi}^{opt}$ is calculated.

Optimize $\boldsymbol{a}$ and fix ($\boldsymbol{\Phi}$, $\boldsymbol{\zeta}$, $\boldsymbol{a}$)

Given fixed RIS precoding matrix $\boldsymbol{\Phi}$ and auxiliary variables $\boldsymbol{\zeta}$ and $\boldsymbol{\kappa}$, the optimization problem in (7) is now expressed as

$$\max_{\boldsymbol{a}} \Re\{\boldsymbol{\varrho}^{\boldsymbol{T}}\boldsymbol{a}\} - \boldsymbol{a}^T\boldsymbol{\Gamma}\boldsymbol{a} \tag{19a}$$

$$s.t. \boldsymbol{a}^T\boldsymbol{\Upsilon}\boldsymbol{a} \leq P_{RIS_{max}} - ||\boldsymbol{\Phi}||^2\sigma_v^2 \tag{19b}$$

$$\sum_{i=1}^{Q}a_i^2 \leq P_{T_{max}} \tag{19c}$$

$$0 \leq a_i, \forall i \in 1,...,Q. \tag{19d}$$

Algorithm 1: Lagrangian Multiplier with Binary Search Method

Input: Channels $\boldsymbol{g}_i$ and $\boldsymbol{f}_i$ $\forall i \in \{1, ..., Q\}$
Output: Active RIS Precoding Matrix $\boldsymbol{\phi}$
Initialize: $\mu^l = 0, \mu^u = 10$
$\boldsymbol{\phi}^l = (\boldsymbol{\Delta} + \mu^l \boldsymbol{\Lambda})^{-1} \boldsymbol{B}^H$, $\boldsymbol{\phi}^u = (\boldsymbol{\Delta} + \mu^u \boldsymbol{\Lambda})^{-1} \boldsymbol{B}^H$.
$P^l = {\boldsymbol{\phi}^l}^H \Lambda \boldsymbol{\phi}^l$, $P^u = {\boldsymbol{\phi}^u}^H \Lambda \boldsymbol{\phi}^u$.
if $P^l < P_{RIS_{max}}$ **then**
  $\boldsymbol{\phi}^{opt} = \boldsymbol{\phi}^l$
while $P^l > P_{RIS_{max}}$ & $P^u > P_{RIS_{max}}$ **do**
  $\mu^l = \mu^u$;
  $\mu^u = 10\mu^u$;
  $\boldsymbol{\phi}^l = (\boldsymbol{\Delta} + \mu^l \boldsymbol{\Lambda})^{-1} \boldsymbol{B}^H$
  $\boldsymbol{\phi}^u = (\boldsymbol{\Delta} + \mu^u \boldsymbol{\Lambda})^{-1} \boldsymbol{B}^H$;
  $P^l = {\boldsymbol{\phi}^l}^H \Lambda \boldsymbol{\phi}^l$;
  $P^u = {\boldsymbol{\phi}^u}^H \Lambda \boldsymbol{\phi}^u$;
while $|\mu^l - \mu^u| > 10^{-5}$ **do**
  $\mu^m = \frac{\mu^l + \mu^u}{2}$;
  $\boldsymbol{\phi}^m = (\boldsymbol{\Delta} + \mu^m \boldsymbol{\Lambda})^{-1} \boldsymbol{B}^H$
  $P^m = {\boldsymbol{\phi}^m}^H \Lambda \boldsymbol{\phi}^m$;
  if $P^m < P_{RIS_{max}}$ **then**
    $\mu^u = \mu^m$
    $\boldsymbol{\phi}^u = (\boldsymbol{\Delta} + \mu^u \boldsymbol{\Lambda})^{-1} \boldsymbol{B}^H$
    $P^u = {\boldsymbol{\phi}^u}^H \Lambda \boldsymbol{\phi}^u$ **else if** $P^m > P_{RIS_{max}}$ **then**
      $\mu^l = \mu^m$
      $\boldsymbol{\phi}^l = (\boldsymbol{\Delta} + \mu^l \boldsymbol{\Lambda})^{-1} \boldsymbol{B}^H$
      $P^l = {\boldsymbol{\phi}^l}^H \Lambda \boldsymbol{\phi}^l$
      else
        $\boldsymbol{\phi}^{opt} = \boldsymbol{\phi}^m$
        break;
  $\boldsymbol{\phi}^{opt} = \boldsymbol{\phi}^u$;
Return $\boldsymbol{\phi}^{opt}$.

where

$$\varrho_i = 2\kappa_i^* \sqrt{1+\zeta_i} (\boldsymbol{f}_i^H \boldsymbol{\Phi} \boldsymbol{g}_i); \tag{20a}$$

$$\boldsymbol{\varrho} = [\varrho_1, ..., \varrho_N]^T; \tag{20b}$$

$$\boldsymbol{\Gamma} = diag(\sum_{\substack{i \in Q \\ j \neq i}}^{Q} |\kappa_j \boldsymbol{f}_j \boldsymbol{\Phi} \boldsymbol{g}_i|^2); \tag{20c}$$

$$\Upsilon = \boldsymbol{\Omega}^H (\boldsymbol{I_Q} \otimes \boldsymbol{\Phi}^{\boldsymbol{H}}) (\boldsymbol{I_Q} \otimes \boldsymbol{\Phi}) \boldsymbol{\Omega}; \tag{20d}$$

$$\boldsymbol{\Omega} = \begin{bmatrix} \boldsymbol{g_1^H} & \boldsymbol{0_N} & ... & \boldsymbol{0_N} \\ \boldsymbol{0_N} & \boldsymbol{g_2^H} & \dots & \boldsymbol{0_N} \\ \boldsymbol{0_N} & \boldsymbol{0_N} & ... & \boldsymbol{0_N} \\ \boldsymbol{0_N} & \boldsymbol{0_N} & \boldsymbol{0_N} & \boldsymbol{g_Q^H} \end{bmatrix}^H_{QN \times Q} \tag{20e}$$

It is noted that problem (19) is also a QCQP problem. Since $a_i, \forall i \in Q$ are all positive semidefinite, then problem (19) is convex and it is solved easily using CVX. Algorithm 2 summarizes the joint power allocation and RIS precoding matrix scheme.

Algorithm 2: Proposed Joint Power Allocation and RIS Precoding Matrix Algorithm

Input: Channels $\boldsymbol{g_i}$ and $\boldsymbol{f_i}$ $\forall i \in \{1, ..., Q\}$.
Output: Optimized users transmit powers $\boldsymbol{a^2}$,
Active RIS Precoding Matrix $\boldsymbol{\Phi}$ and Sum Rate R_{sum}.
Randomly initialize $\boldsymbol{a}$ **and** $\boldsymbol{\Phi}$,
while R_{sum} *does not converge* **do**
  Update $\boldsymbol{\zeta}$ using (11);
  Update $\boldsymbol{\kappa}$ using (13);
  Update $\boldsymbol{\phi}$ by solving (18) using Algorithm 1;
  Update $\boldsymbol{a}$ by solving (19) using CVX;
Return Optimized $\boldsymbol{a}$, $\boldsymbol{\Phi}$ and R_{sum}.

VI. Performance Evaluation and Numerical Results

In this section, the performance of the proposed joint power allocation and active RIS precoding matrix optimization scheme is evaluated using Matlab R2021b and compared with two other schemes, passive-RIS aided network and multi-antenna AF relaying scheme. Optimum power allocation in addition to optimum RIS precoding matrices are used in passive and active RIS. For the AF scheme, the total system power budget P_{max} is divided equally among transmitting devices and every transmitting device is assigned P_{AF}, where $P_{AF} = \frac{P_{max}}{Q}$.

The received signal in case of the multi-antenna relaying scheme at user i is expressed as

$$y_{i_{AF}} = (\boldsymbol{G}_{AF} \odot \boldsymbol{f}_i^H) \boldsymbol{g}_i \sqrt{P_{AF}} x_i$$
$$+ (\boldsymbol{G}_{AF} \odot \boldsymbol{f}_i^H) \boldsymbol{n}_r + \sum_{\substack{j=1 \\ j \neq i}}^{Q} \sqrt{P_{AF}} h_j + n_o;$$

where $\boldsymbol{G}_{AF} = [G_1, G_2, ...G_N] \in \mathbb{C}^{1 \times N}$ and G_i is expressed as

$$G_i = \sqrt{\frac{P_{AF}}{P_{AF}|g_i|^2 + N_o}}.$$

$\odot$ represents element-to-element multiplication, h_j represents the channel gain of interferer j at receiver i and $\boldsymbol{n}_r \in \mathbb{C}^{N \times 1}$ is the AWGN noise generated at the AF relay.

The effect of varying some parameters such as distances between the MD and the RIS, the number of RIS elements N, the number of underlying D2D pairs M and the system available power budget P_{max} on the performance of the algorithm is studied. We assume a square area for the deployment of all links with an edge of 70 m. The values of the simulation parameters are summarized in Table I.

In Fig.2, the achieved sum rate of the three schemes is plotted versus the distance between the MD and UAV equipped with the RIS, where all other nodes are kept constant. For fair comparison, the same total system power budget P_{max} is assigned to the three schemes. As the figure depicts, increasing the distance between the MD and the UAV results in a degradation in the achieved sum rate for the three schemes. Indeed, this is due to the higher pathloss of the THz wave.

TABLE I: Simulation Parameters.

Parameter	Description	Value
f	Operating frequency	1 THz
$k(f)$	Absorption coefficient	0.1
G_{Tx}	Transmitting node Gain	30 dB
G_{Rx}	Receiving node Gain	10 dB
N	Number of antenna elements (in RIS or AF Relay)	100
M	Number of D2D Pairs	3
N_o, σ_v^2	Noise variance	-80 dB
P_{max}	Total System Power Budget	10 W
$P_{RIS_{max}}$	RIS Power Budget	5 W
$P_{T_{max}}$	Transmitting nodes' Maximum Power	5 W
W	System available BW	10^8

Moreover, the proposed joint power allocation and active RIS precoding matrix optimization scheme achieves the highest sum rate among the three schemes, followed by the passive RIS-assisted network and then the AF scheme which achieves the lowest performance among them. This implies that using active RIS improves the performance compared to AF relaying scheme. This is because active RIS that does not only amplify the incident signals like AF does, but also adjusts the signals' phases in a favorable matter so that the unwanted phases added by the channel are eliminated.

In Fig.3, the achieved sum rate of the three schemes is plotted versus the number of underlying D2D pairs M. From the figure, for the three schemes, as the number of D2D devices increases, the achieved sum rate decreases, where the decreasing rate is very significant in the active RIS scheme compared to the passive RIS and the AF scheme. These falling-off rates are due to the significant interference from undesired users that can be sensed at each user. Furthermore, it is denoted that the active RIS scheme achieves remarkably the highest sum rate,

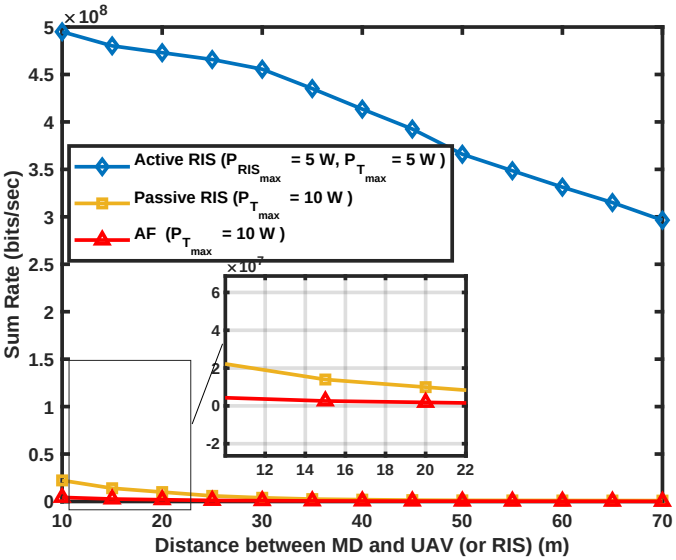

Fig. 2: Sum Rate versus Distance for the three Schemes (Active RIS, Passive RIS and AF Scheme).

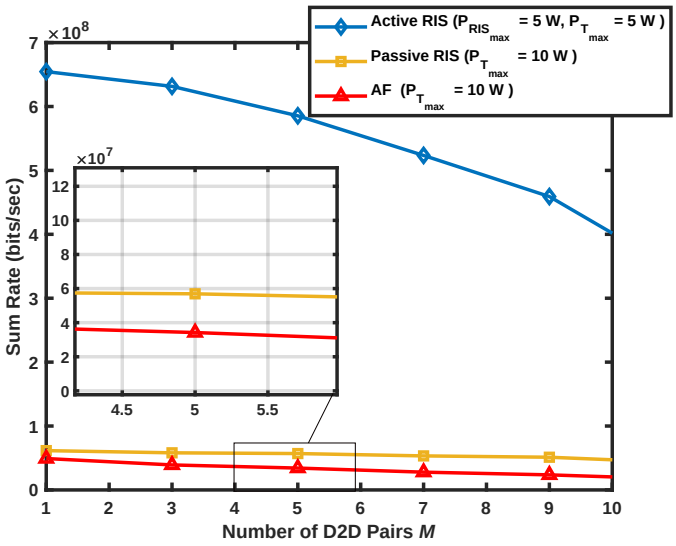

Fig. 3: Sum Rate versus Number of D2D Devices M for the three Schemes (Active RIS, Passive RIS and AF Scheme).

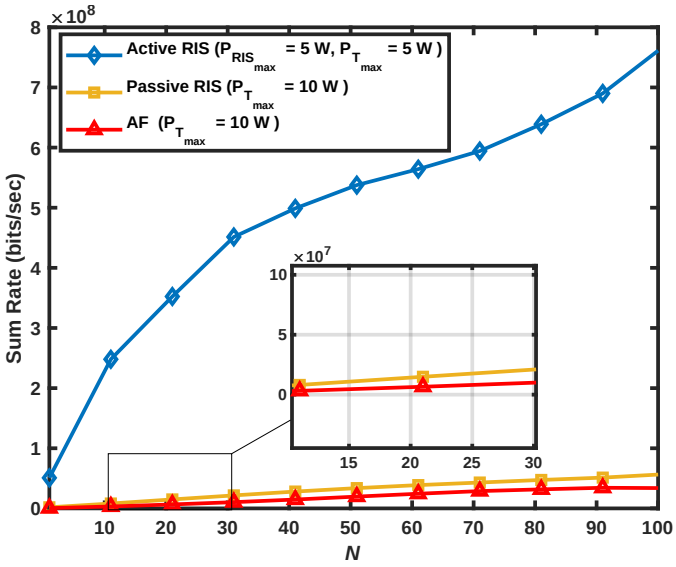

Fig. 4: Sum Rate versus number of RIS elements or AF relay elements N for the three Schemes (Active RIS, Passive RIS and AF Scheme).

then comes the passive RIS scheme and the AF scheme, which almost have very close performance especially at small values of M.

In Fig.4, the achieved sum rate of the three schemes is plotted versus N. As mentioned before, N is the number of RIS elements which is also the number of antennas of AF relay. As the figure depicts, increasing N results in an increase in all schemes. It is also shown that the performance of the passive RIS scheme is a bit higher than that achieved by the AF scheme. This is because the passive RIS scheme reconfigures the incident signal phases so that destructive phase shifts added by the channels are removed. In addition, the AF scheme unintentionally amplifies the noise signal which results

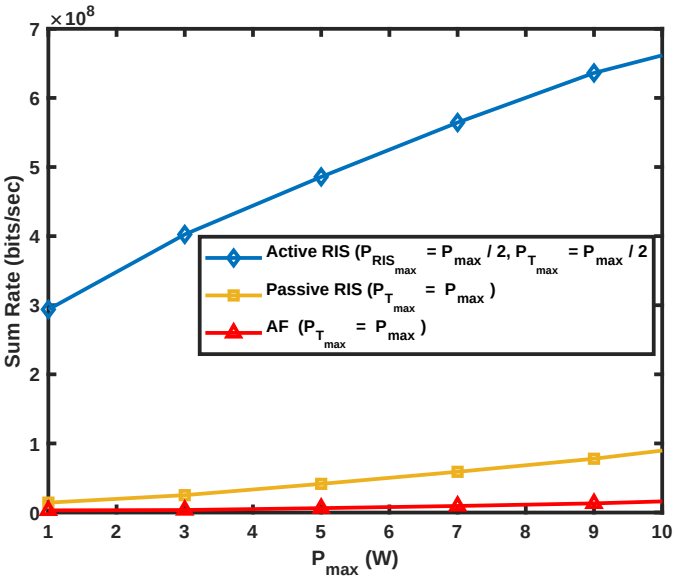

Fig. 5: Sum Rate versus the total system power budget P_M for the three Schemes (Active RIS, Passive RIS and AF Scheme).

in a deterioration in the received signal quality, achieving the lowest performance.

In Fig.5, the achieved sum rate of the three schemes is plotted versus the total system power budget P_{max}. As expected, increasing the total system power budget results in an increase in the achieved sum rate. This is because the increase of P_{max} allows higher transmit power for the MD and the D2D transmitting devices which results in a gradual increase in the sum rate. In addition, the figure indicates that the highest sum rate is achieved by the active RIS assisted network followed by the passive RIS-assisted system and eventually comes the AF scheme. This implies that the active RIS scheme well-invests its assigned power budget among transmitting users and reflecting active RIS coefficients so that the total sum rate is enhanced.

VII. Conclusions and Future Works

In this paper, the sum rate of an uplink active RIS- and UAV-assisted one cell communication system is considered, in the existence of some underlying D2D devices. A joint power allocation and active RIS precoding matrix optimization scheme is proposed to maximize the sum rate. Accordingly, the sum rate optimization problem is formulated accordingly with power constraints are taken into consideration. Numerical results show the superiority of deploying active RIS in the network to boost communication compared to deploying passive RIS as well as multi-antenna AF relaying scheme. For instance, inspecting the proposed scheme deploying active RIS at different distances, various number of underlying D2D devices, more total system power budget and for different RIS elements, the proposed scheme surpasses its counterparts, achieving significantly the highest sum rate. For future work, considering the mobility of the UAV is the current focus of the authors' work.

References

[1] Z. Zhang, L. Dai, X. Chen, C. Liu, F. Yang, R. Schober, and H. V. Poor, "Active ris vs. passive ris: Which will prevail in 6g?" *arXiv preprint arXiv:2103.15154*, 2021.

[2] G. C. Alexandropoulos, G. Lerosey, M. Debbah, and M. Fink, "Reconfigurable intelligent surfaces and metamaterials: The potential of wave propagation control for 6g wireless communications," *arXiv preprint arXiv:2006.11136*, 2020.

[3] C. Molero, Á. Palomares-Caballero, A. Alex-Amor, I. Parellada-Serrano, F. Gamiz, P. Padilla, and J. F. Valenzuela-Valdés, "Metamaterial-based reconfigurable intelligent surface: 3d meta-atoms controlled by graphene structures," *IEEE Communications Magazine*, vol. 59, no. 6, pp. 42–48, 2021.

[4] E. Björnson, H. Wymeersch, B. Matthiesen, P. Popovski, L. Sanguinetti, and E. de Carvalho, "Reconfigurable intelligent surfaces: A signal processing perspective with wireless applications," *IEEE Signal Processing Magazine*, vol. 39, no. 2, pp. 135–158, 2022.

[5] L. Dong, H.-M. Wang, and J. Bai, "Active reconfigurable intelligent surface aided secure transmission," *IEEE Transactions on Vehicular Technology*, vol. 71, no. 2, pp. 2181–2186, 2021.

[6] K. Liu, Z. Zhang, L. Dai, S. Xu, and F. Yang, "Active reconfigurable intelligent surface: Fully-connected or sub-connected?" *IEEE Communications Letters*, vol. 26, no. 1, pp. 167–171, 2021.

[7] Z. Peng, X. Liu, C. Pan, L. Li, and J. Wang, "Multi-pair d2d communications aided by an active ris over spatially correlated channels with phase noise," *IEEE Wireless Communications Letters*, 2022.

[8] S. Farrag, E. Maher, A. El-Mahdy, and F. Dressler, "Outage probability analysis of uav assisted mobile communications in thz channel," in *IEEE/IFIP WONS 2021*. IEEE, 2021, pp. 1–8.

[9] ——, "Performance analysis of uav assisted mobile communications in thz channel," *IEEE Access*, vol. 9, pp. 160 104–160 115, 2021.

[10] A. Alali, D. B. Rawat, and C. Liu, "Trajectory and power optimization in sub-thz band for uav communications," in *IEEE ICC 2022*. IEEE, 2022, pp. 1–6.

[11] M. M. Azari, F. Rosas, and S. Pollin, "Cellular connectivity for uavs: Network modeling, performance analysis, and design guidelines," *IEEE Transactions on Wireless Communications*, vol. 18, no. 7, pp. 3366–3381, 2019.

[12] M. Tesanovic and M. Nekovee, "mmwave-based mobile access for 5g: key challenges and projected standards and regulatory roadmap," in *IEEE GLOBECOM 2015*. IEEE, 2015.

[13] J. M. Eckhardt, V. Petrov, D. Moltchanov, Y. Koucheryavy, and T. Kürner, "Channel measurements and modeling for low-terahertz band vehicular communications," *IEEE Journal on Selected Areas in Communications*, vol. 39, no. 6, pp. 1590–1603, 2021.

[14] C. Han and Y. Chen, "Propagation modeling for wireless communications in the terahertz band," *IEEE Communications Magazine*, vol. 56, no. 6, pp. 96–101, 2018.

[15] R. Wang, Y. Mei, X. Meng, and J. Ma, "Secrecy performance of terahertz wireless links in rain and snow," *Nano Communication Networks*, vol. 28, p. 100350, 2021.

[16] H. Zhang, H. Zhang, W. Liu, K. Long, J. Dong, and V. C. Leung, "Energy efficient user clustering, hybrid precoding and power optimization in terahertz mimo-noma systems," *IEEE Journal on Selected Areas in Communications*, vol. 38, no. 9, pp. 2074–2085, 2020.

[17] Y. Liu, W. Li, and Z. Lin, "A dynamic subarray structure in reconfigurable intelligent surfaces for terahertz communication systems," *arXiv preprint arXiv:2206.14968*, 2022.

[18] C. Huang, Z. Yang, G. C. Alexandropoulos, K. Xiong, L. Wei, C. Yuen, and Z. Zhang, "Hybrid beamforming for ris-empowered multi-hop terahertz communications: A drl-based method," in *IEEE GLOBECOM 2020, Workshops*. IEEE, 2020.

[19] A.-A. A. Boulogeorgos, E. N. Papasotiriou, and A. Alexiou, "A distance and bandwidth dependent adaptive modulation scheme for thz communications," in *IEEE SPAWC 2018*. IEEE, 2018.

[20] J. M. Jornet and I. F. Akyildiz, "Channel Modeling and Capacity Analysis for Electromagnetic Wireless Nanonetworks in the Terahertz Band," *IEEE Transactions on Wireless Communications*, vol. 10, no. 10, pp. 3211–3221, Oct. 2011.

[21] K. Shen and W. Yu, "Fractional programming for communication systems—part i: Power control and beamforming," *IEEE Transactions on Signal Processing*, vol. 66, no. 10, pp. 2616–2630, 2018.